Journal of Crystallization Process and Technology, **2012, 2, 1-11**
http://dx.doi.org/10.4236/jcpt.2012.21001 Published Online January 2012 (http://www.SciRP.org/journal/jcpt)

Determination of A.C. Conductivity of Nano-Composite Perovskite $Ba_{(1-x-y)}Sr_{(x)}TiFe_{(y)}O_3$ Prepared by the Sol-Gel Technique

M. Willander[1], O. Nur[1], M. Q. Israr[1], A. B. Abou Hamad[2], F. G. El Desouky[2], M. A. Salem[2], I. K. Battisha[2*]

[1]Department of Science and Technology, Campus Norrkoping, Linkoping University, Norrkoping, Sweden; [2]Solid State Physics Department, National Research Center (NRC), Giza, Egypt.
Email: [*]szbasha@yahoo.com

Received September 15th, 2011; revised October 25th, 2011; accepted November 6th, 2011

ABSTRACT

Nano-composite, perovskite $Ba_{(1-x-y)}Sr_{(x)}TiFe_{(y)}O_3$, denoted as (BSTF) in powder form was derived via sol-gel (SG) method followed by sintering at fixed temperature 750˚C for one hour. The morphology and structure of the powder samples were investigated by using X-ray diffraction (XRD), transmission electron microscope (TEM) and scanning electron microscope (SEM). The XRD characterization indicates formation of a tetragonal crystalline phase in the pure BST. A well defined perovskite phase with nano-crystallite sizes equal to about 32 nm was achieved from XRD for B10ST20F sample, while TEM study confirmed the obtained XRD results giving the following crystallite size value about 29.82 nm for the same sample. The dielectric A.C. conductivity was evaluated as a function of temperature and frequency ranging from 42 Hz up to 1 MHz.

Keywords: Sol-Gel; Dielectric Permittivity; A.C. Conductivity; Nano-Structure $BaSrTiO_3$ (BST); TEM; XRD and SEM

1. Introduction

Barium titanate, which is the host material for doping with the Sr has been extensively employed in several industrial applications, including dynamic random access memory (DRAM) capacitors, microwave filters, infrared detectors and dielectric phase shifters, due to its excellent ferroelectric, dielectric, piezoelectric and pyroelectric properties [1-5]. It was previously reported that for the ABO_3 perovskite, different A-site and B-site dopants (where A = Ca, Sr, La; B = Nb, Ta, Zr) were used to modify the electrical properties of $BaTiO_3$ based compositions [6-9].

Recently, barium strontium titanate (BST) attracted much attention because of its strong dielectric nonlinearity under bias electric field and linearly adjustable Curie temperature with the strontium content over a wide temperature range [9-11]. The desired properties make BST a promising candidate material for tunable microwave dielectric devices [12,13]. Ferroelectric and dielectric properties of BST ceramics are strongly dependent on the sintering conditions, grain size, porosity, doping amount and structural defects [14-16].

Fe-doped $(Ba_{1-x}Sr_x)TiO_3$ is usually prepared by many processes such as ball milling, solid-state reaction and sol gel, which is used in this work etc. either in powder or thin film forms. It was suggested previously that in Fe-doped $(Ba_{1-x}Sr_x)TiO_3$ micro-structural and dielectric properties were modified by controlling the Fe concentration ($0.01 \leq x \leq 0.20$ mol%) with fixed Sr concentrations [1-8]. Barium strontium titanate (BST) with high dielectric constant (ε) attracted much interest as materials for environmentally applications (dielectric for capacitors, actuators, etc.). It is a perovskite-based ferroelectric, and one of the most studied ferroelectric materials, exhibiting normal, first-order phase transition behavior. Previous studies on the dielectric properties of $Ba_xSr_{1-x}TiO_3$ ceramic solid solutions have shown that the compositions with $x \geq 0.2$ exhibited normal ferroelectric behavior while the relaxation characteristics have been observed in the $SrTiO_3$ rich region ($x < 0.2$). The loss factor in these materials is reduced with the addition of a proper substitute. Few authors have reported the substitution of Fe in BST and strontium titanate where Fe^{3+} ion substitutes Ti^{4+} in BST and reduces the dissipation factor due to domain wall motion [9-20].

The purpose of the present work is to determine the temperature and the frequency dependence on dielectric and A.C. conductivity of the prepared nano-composite BST and BSTF powders samples. The structure and the morphology of the prepared samples will be evaluated by

[*]Corresponding author.

using XRD, SEM and TEM.

2. Materials and Methods

2.1. Samples Preparation

$Ba_{(1-x)}Sr_{(x=0.1)}TiO_3$ and $Ba_{(1-x-y)}Sr_{(x)}TiFe_{(y)}O_3$ where (x = 0.1 and y = 0.01, 0.03, 0.05, 0.15 & 0.20) denoted as (BST) and BST(1 - 0.20)F, respectively powder systems were prepared by a modified sol-gel method. BST system has the following different Sr contents and symbols: (a) B3ST = 0.03 mol% Sr, B10ST= 0.1 mol% Sr, B15ST = 0.15 mol% Sr and B20ST = 0.2 mol% Sr. While the $Ba_{(1-x-y)}Sr_{(x)}TiFe_{(y)}O_3$, where (x = 0.1 and y = 0.01, 0.03, 0.05, 0.10, 0.15 & 0.20) has the following different Fe contents and symbols, (a) B10ST1F = 0.1 mol% Sr & 0.01 mol% Fe, (b) B10ST3F = 0.1 mol% Sr & 0.03 mol% Fe, (c) B10ST5F = 0.1 mol% Sr & 0.05 mol% Fe, (d) B10ST10F = 0.1 mol% Sr & 0.1 mol% Fe and (e) B10ST20F = 0.1 mol% Sr & 0.20 mol% Fe, respectively.

$BaSrTiO_3$ doped with different concentrations of strontium and iron in powder form have been prepared using barium acetate ($Ba(Ac)_2$) (99%, Sisco Research Laboratories PVT.LTD, India) and titanium butoxide ($Ti(C_4H_9O)_4$), (97%, Sigma-Aldrich, Germany) as starting materials. Acetyl acetone (AcAc, $C_5H_8O_2$), (98%, Fluka, Switzerland) acetic acid (HAc)-H_2O mixture (96%, Adwic, Egypt) were adopted as solvents of ($Ti(C_4H_9O)_4$), and $Ba(Ac)_2$, respectively. Strontium bromide was added to the precursor with different molar ratios. Iron nitrate was added to the final solution of B10ST with different concentrations. Densification of the gel was achieved by sintering in air for one hour at 750˚C, in a muffle furnace type (Carbolite CWF 1200).

2.2. Characterization

X-ray diffraction (XRD) patterns were recorded with a Philips X-ray diffractometer using monochromatic $CuK_{\alpha 1}$ radiation of wavelength λ = 1.5418 Å from a fixed source operated at 40 kV and 30 mA. The crystallite size (G) was determined from the Scherrer's equation $G = K\lambda/D\cos\theta$, where K is the Scherer constant (0.9), λ is the wavelength and D is the full width (in radians) of the peak at half maximum (FWHM) intensity.

The microstructure and the morphology of the prepared samples were characterized by using JEOL transmission electron microscope (TEM), model: Jeol 1230" with magnification up to 600 k×, giving a resolution down to 0.2 nm. We performed the measurement at an accelerating voltage of 100 kV. A computerized LRC bridge (Hioki model 3531 Z Hi Tester) was used to measure the electrical properties of the samples. The dielectric constant $\in$ for the investigated samples was studied from room temperature up to 250˚C at different frequencies ranging from 42 Hz up to 1 MHz. The samples used in the dielectric measurements were in disk form, having 10 mm in diameter and 3 mm in thickness, pressed using a pressure of 10 Ton at room temperature. Then, silver paste was coated to form electrodes on both sides of the sintered ceramic specimens in order to ensure good contacting. The electrical measurements were carried out by inserting the sample between two parallel plate conductors forming cell capacitor. Then, the whole arrangement was placed in to non-inductive furnace for heating the samples with constant rate [1].

$$\varepsilon' = \frac{Cd}{\varepsilon_0 A} \tag{1}$$

$$\varepsilon\varepsilon'' = \varepsilon' \tan\delta \tag{2}$$

where, ε' is the permittivity, ε'' is the dielectric loss and tanδ is the loss tangent and A is the area of the electrode.

The A.C. resistivity of the prepared samples was estimated from the dielectric parameters. As long as the pure charge transport mechanism is the major contributor to the loss mechanism, the resistivity (ρ) can be calculated using the following relation:

$$(\rho) = 1/(\omega\,\varepsilon_0'\varepsilon'\tan\delta)\ \Omega\,\mathrm{Cm} \tag{3}$$

where $\omega = 2\pi f$, ω is the angular frequency and f is the frequency of the applied electric field in Hertz.

$$s = 2\pi\,fdC\tan\delta/A \tag{4}$$

where σ is the A.C. conductivity, f is the operating frequency, d is the thickness of the dielectrics, tanδ is the dielectric loss, C is the capacitance and A is the area of the electrode.

3. Results and Discussion

X-ray diffraction was performed to characterize the crystallinity and phase of the nano-particles. **Figures 1** and **2** show the XRD patterns of pure BS10T and BST5&20Fe, respectively. The XRD patterns indicate that all the samples are polycrystalline and exhibit tetragonal perovskite structure with (110) as a major peak, (JPCDS No 44-0093). The inset in **Figure 1** shows the splitting in the peak extended in the range between $2\theta^\circ$ equal 43.5 and 47 which, is consistent with the tetragonal phase.

Figure 2 shows the XRD patterns of BST5&20F, sintered for one hour at 750˚C. New hematite phase α—Fe_2O_3 was began to appear in the B10ST20F pattern.

Figure 3 shows the splitting of the peak in the 2θ range between 43.5˚ and 47˚, which was shifted towards a lower $2\theta^\circ$ value by increasing the iron oxide concentration. The splitting was appeared well in B10ST5F sample while it began to be weaker in B10ST20F sample but the tetragonal phase is still present in it. The obtained data imply the presence of the tetragonal structure phase from XRD in pure BST and B10ST5&20F samples, Card

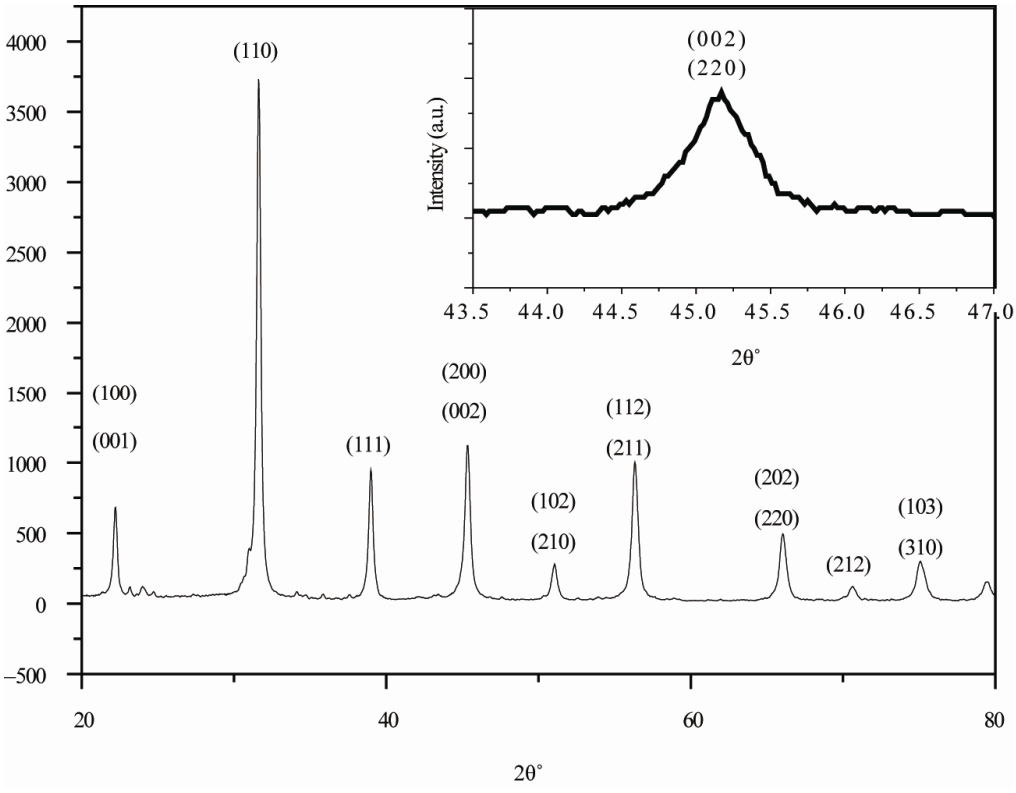

Figure 1. XRD patterns of B10ST powder samples sintered at 750˚C for 1 hour, the inset is of the expansion of the angle 2θ˚ ranges between 43.5˚ up to 47˚, respectively.

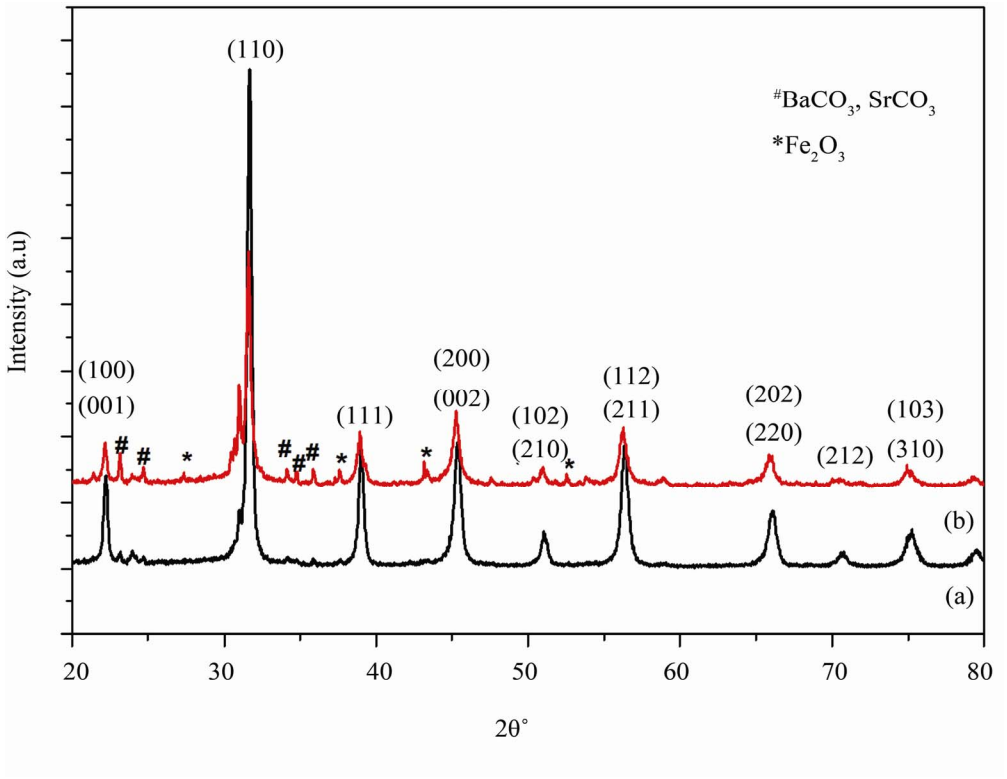

Figure 2. XRD patterns of (a) B10ST5F and (b) B10ST20F powders s samples sintered for one hour at 750˚C for one hour.

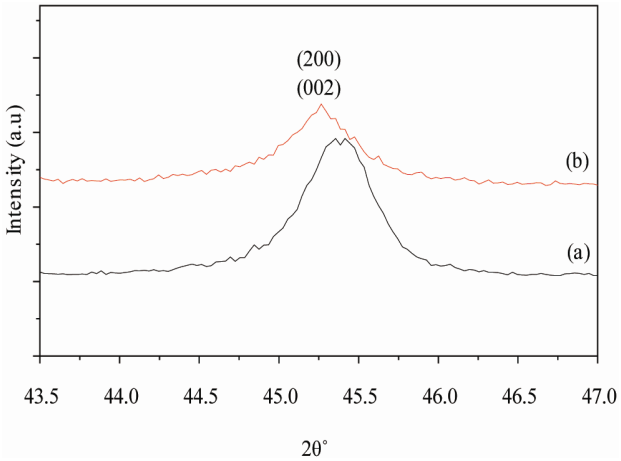

Figure 3. The expansion of the $2\theta^{\circ}$ in the range between 43.5˚ up to 47˚ of (a) B10ST5F and (b) B10ST20F.

number [44-0093] (tetragonal phase).

Weak lines corresponding to the residual carbonates phases, such as $BaCO_3$, $SrCO_3$ and (Ba, Sr)CO_3 were appeared [16]. The full width at half maximum of (110) peak increases by increasing iron oxide concentration which, indicated the decrease in the crystallite sizes from 36.5 nm for pure B10ST to 33.5 and 32 nm for both doped samples B10ST5F and B10ST20F, respectively. The average crystallite size decreased as the dopand concentration was increased, which could be attributed to the fact that the particle growth was hindered by the oxygen vacancies, lattice distortion as well as the internal stress arising from the substitution of Ti with Fe [18,19].

Figure 4 shows the representative TEM of BS10T20F thermally synthesized in air for 1 h at 750˚C. Some degree of agglomerates has been found in the clusters consisting of many small grains [20,21]. The calculated average crystallite size from TEM was 29.82 nm, which is nearly equal to the value obtained from XRD (32 nm) for the same sample. The TEM was used to confirm the data obtained from XRD patterns and that the sample is in nano-scale.

Surface morphologies obtained through Scanning Electron Microscope (SEM) of the pure B(3, 5 & 0.20)ST and doped samples B10ST(3, 5 & 20) Fe powder samples sin

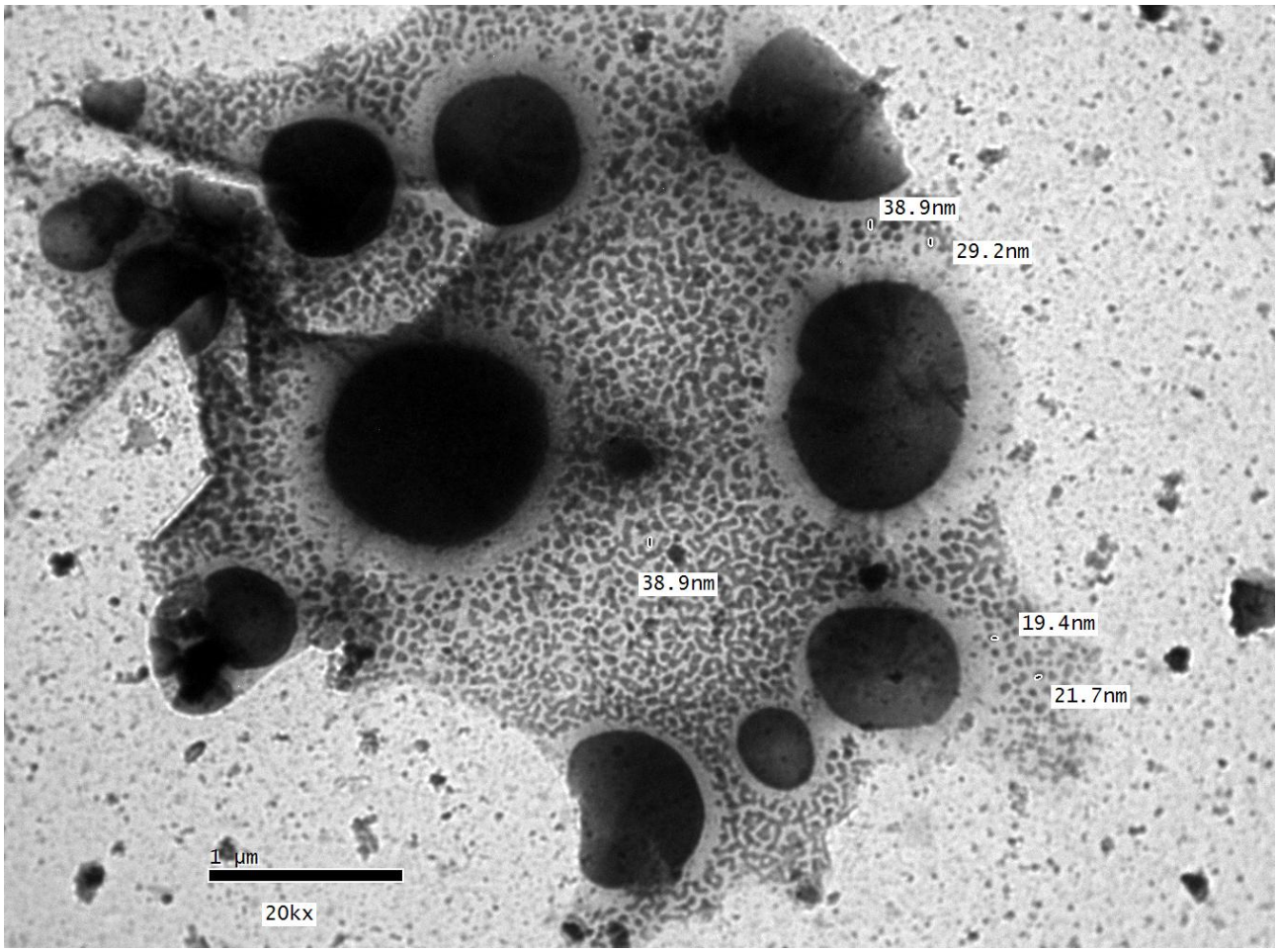

Figure 4. TEM micrographs of B10ST20F, powder samples sintered at 750˚C for one hour.

tered at 750˚C for one hour were shown in **Figures 5(a)-(c)** and **Figures 6(a)-(c)**, respectively. The images in **Figure 5** shows comparatively more accumulated particles with higher density showing increase in grain growth at higher Sr content and the particles have a well-defined shape.

Images in **Figure 6** clearly show that the additive of iron oxide has leads to a grains refining, whereas their lack induce a strong effect of exaggerated grain growth by the formation of large faceted grains, and higher density than the pure samples was observed due to the well dispersion

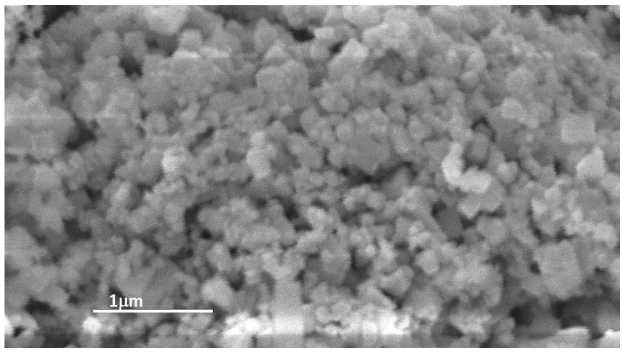

(a)

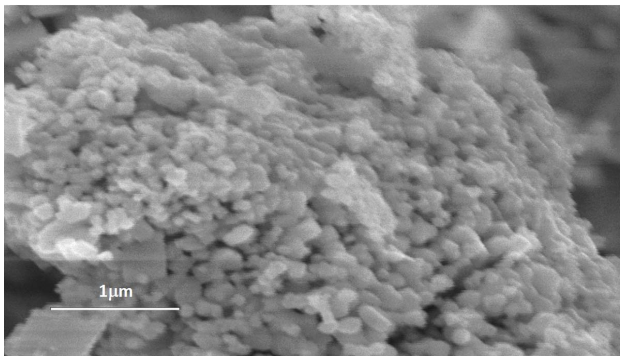

(b)

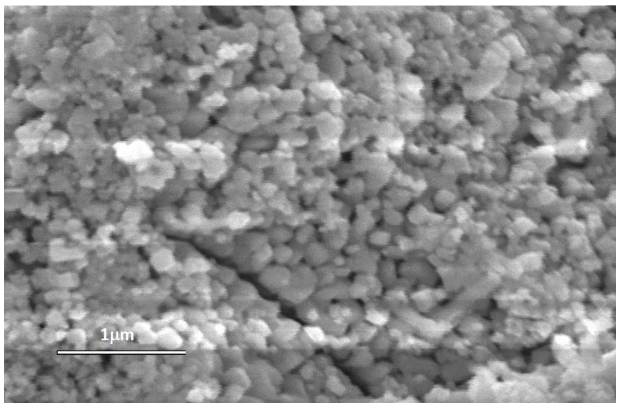

(c)

Figure 5. **The SEM micrograph of (a) (B3ST), (b) (B5ST) and (c) (B20ST) powder samples sintered at 750˚C for one hour.**

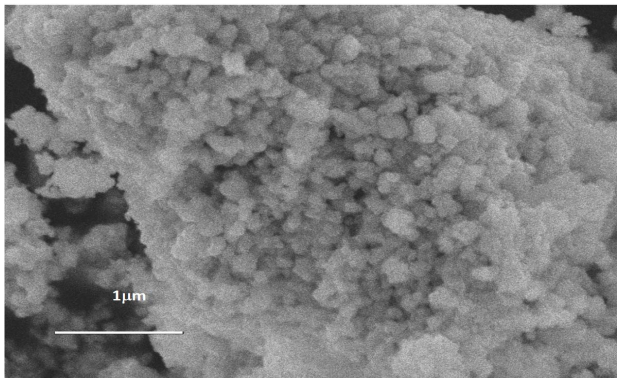

(a)

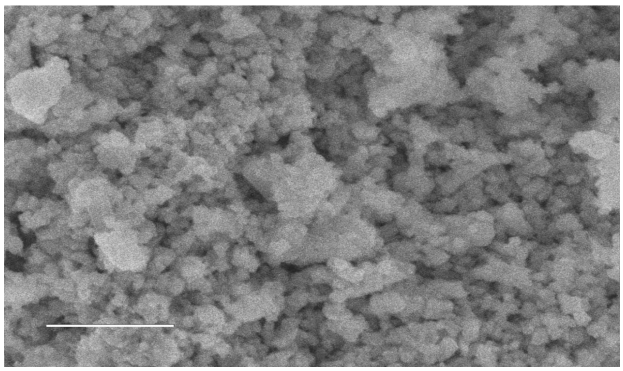

(b)

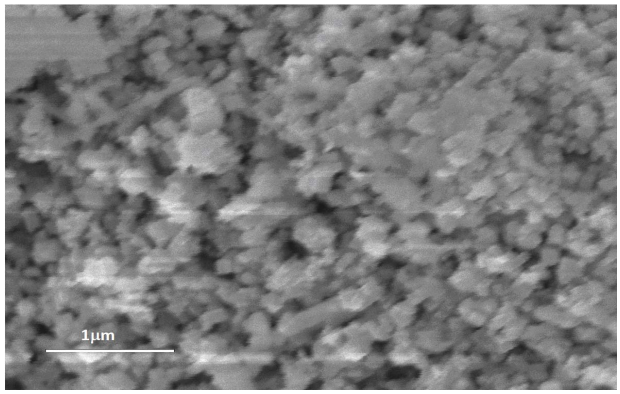

(c)

Figure 6. The SEM micrograph of (a) (B10ST3F), (b) (B10-ST10F) and (c) (B10ST20F) powder samples sintered at 750˚C for one hour.

of iron oxide inside the pure sample. This can be correlated with the predominant XRD peaks as obtained for the doped samples in which new hematite phase appeared at higher iron concentration [19].

To investigate the dielectric properties of our two BST systems (doped and un-doped samples), we fabricated capacitors using silver paste as an electrode. For doped samples B10ST10F and B10ST20F a typical Curie-Weiss response was registered and the temperature dependence of their relative permittivity were shown in **Figures 7(a)** and

(b). It was found that the dielectric constant of each sample has its own maximum corresponding to the Curie point temperature (T_c) where the (T_c) decreases by doping the sample with 10 and 20 mol% of iron oxide giving the following values 80˚C and 50˚C, respectively as shown in **Figures 7(a)** and **(b)** [22] This might be due to phase transformation from the ferroelectric (polarized state) to the para-electric (unpolarized sate).

Figure 8 shows the frequency dependence of the dielectric permittivity ε' (a and c) and the loss tangent tanδ (b and d) of B10ST10F and B10ST20F samples as a function of the frequency during heating in the range starting from 25˚C up to 250˚C. The same behavior from the pure BST system mentioned previously by our team work was observed [16], where the dielectric constant (ε') decreased with increasing frequency showing an anomalous dispersion. Such dispersion in (ε') is accompanied by a relaxation peak in tanδ. The intensity of this peak is slightly increased and its maximum shifted to lower frequencies with increasing the temperature for B10ST10F and B10ST20F. Then it disappeared at a temperature above 70˚C and 50˚C, respectively for the two samples. At these two mentioned temperature, Curie temperature (T_c), abrupt change in dielectric properties can be occurred. Above T_c, (ε') showed markedly decrease leading to ferroelectric-paraelectric phase transition.

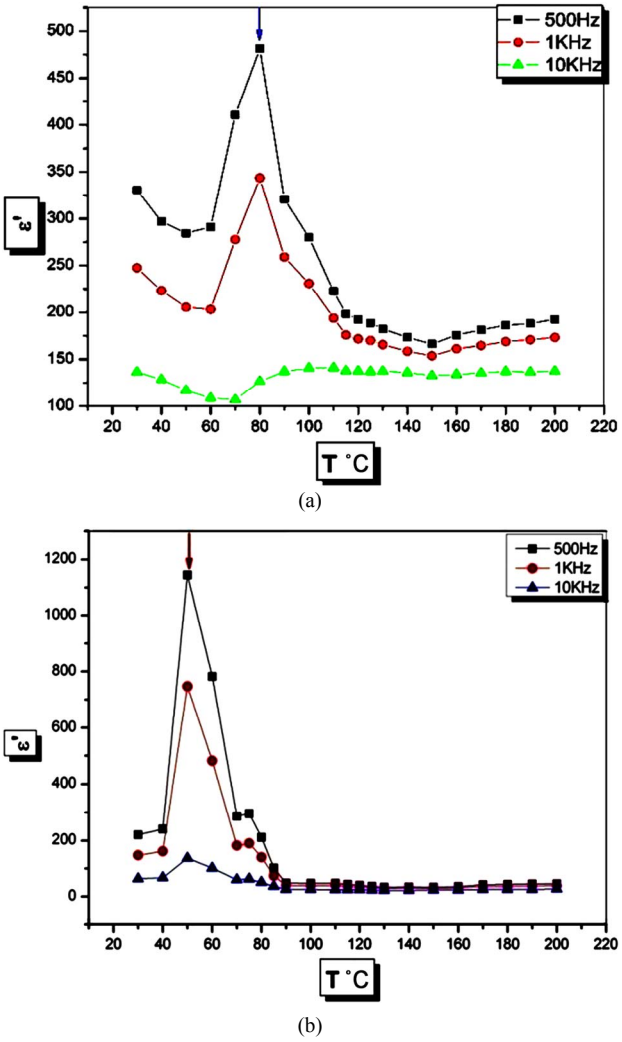

Figure 7. Temperature dependence of the dielectric constant at various frequencies for (a) B10ST10F and (b) B10ST20F.

The Curie temperature of the doped samples were found to be decreased from 80˚C to 50˚C for the doped barium strontium titanate B10ST10F and B10ST20F, respectively, indicating ferroelectric-para-electric phase transition. A notable decrease in dielectric constant by increasing the iron content was observed due to the fact that iron oxide dopants may inhibit grain growth and therefore reduction of grain size was occurred. Consequently, the dielectric properties of the B10ST(10 and 20)F are decreased. Another interpretation for such decrease related to the fact that iron oxide has different lattice constant which add a stress in to the lattice [23-25].

By focusing our study on the A.C conductivity one can observe from **Figure 9** that the A.C. conductivity increases by increasing the frequency values. The conductivity (σ) of the samples was calculated using the formula $\sigma = 2\pi fdC \tan\delta/A$ as shown in Equation (4) Section 2. At 30˚C and 100˚C the A.C. conductivity was found to decrease by increasing the Sr concentration from 10 up to 15 mol%, and by doping with different concentrations of iron oxide, while at 120˚C the doped samples with Sr have higher conductivity as shown in **Table 1**. The decrease in conductivity by doping with different concentrations of Sr and Fe may be primarily due to the decrease in tanδ loss with Sr and Fe substitution as stated earlier [26], or may be partly due to the decrease in the grain size and hence the increase in the grain boundary areas/ resistance with Sr and Fe substitution. Grain boundary areas are highly resistive in oxide ceramics. Smaller grain sized ceramics has a larger grain boundary areas and hence higher resistivity.

This result is consistent with the previously reported results; where it was confirmed that the intrinsic capability of the perovskite structure (ABO_3) to host ions of different sizes, with doping in small amounts with acceptor ions could greatly affect the dielectric properties [27-30]. However, the effect of the specific impurity on the electrical conductivity depends on the substitution site so the trivalent ion like Fe^{3+} behaves as an acceptor when substitution occurs at the Ti site or as a donor when it substitutes at the Ba site. Acceptor dopants are defined as ions with a lower valence than the ions that they replaced (e.g. Fe^{3+} for Ti^{4+}). Chan and Smyth [30] postulated that acceptor impurities are mostly compensated by oxygen vacancies.

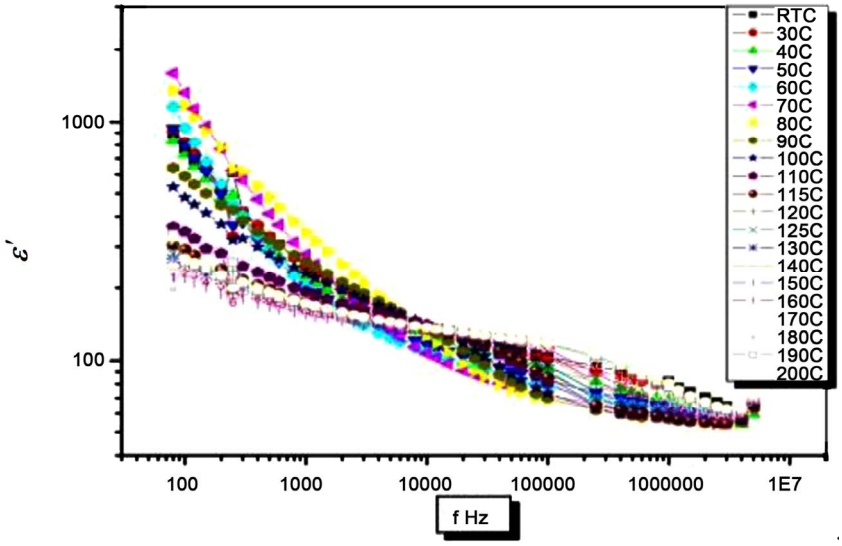

(a)

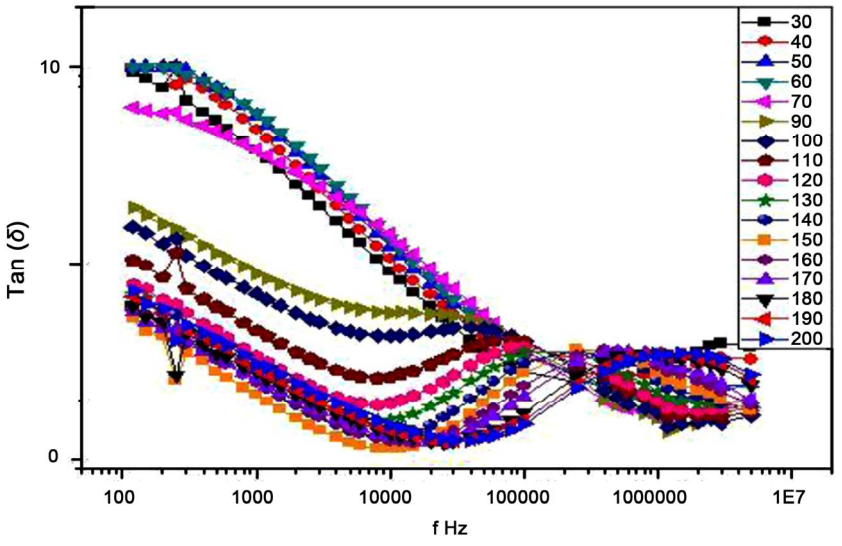

(b)

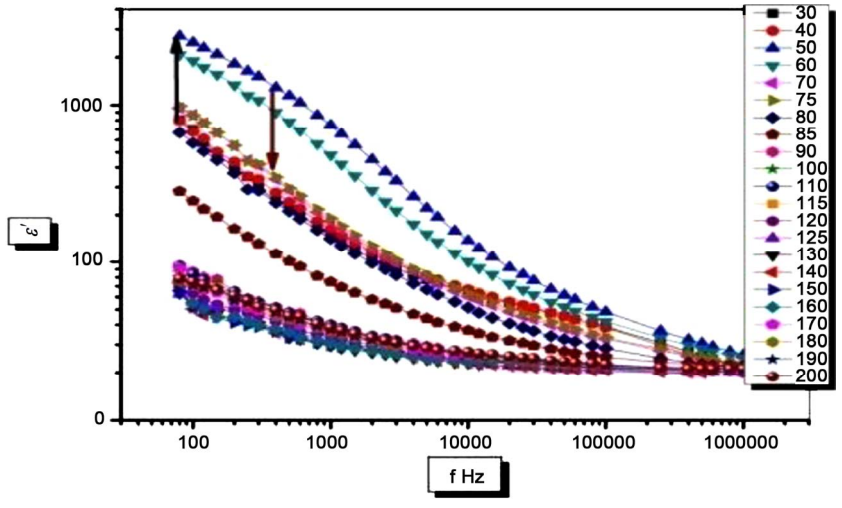

(c)

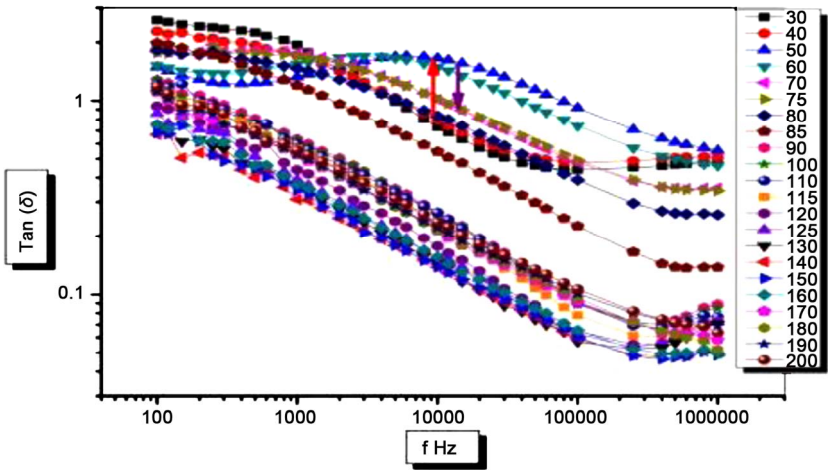

(d)

Figure 8. The frequency dependence of the dielectric permittivity ε' (a and c), and the loss tangent tanδ (b and d) of B10-ST10F and B10ST20F.

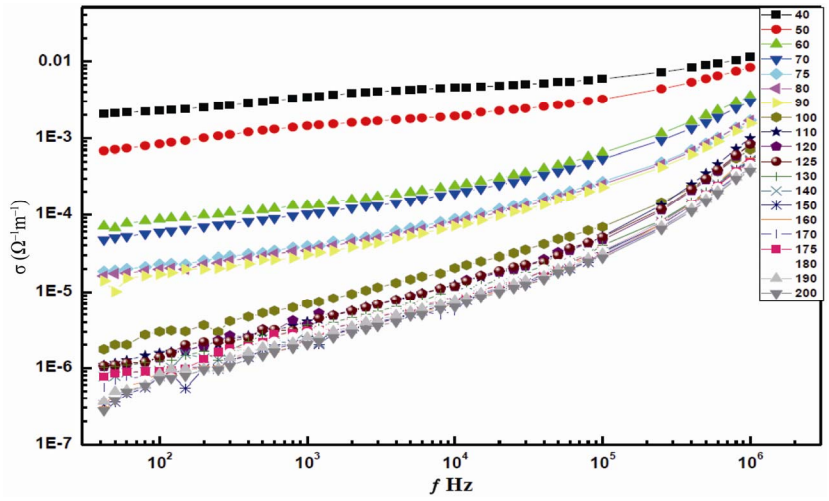

(a)

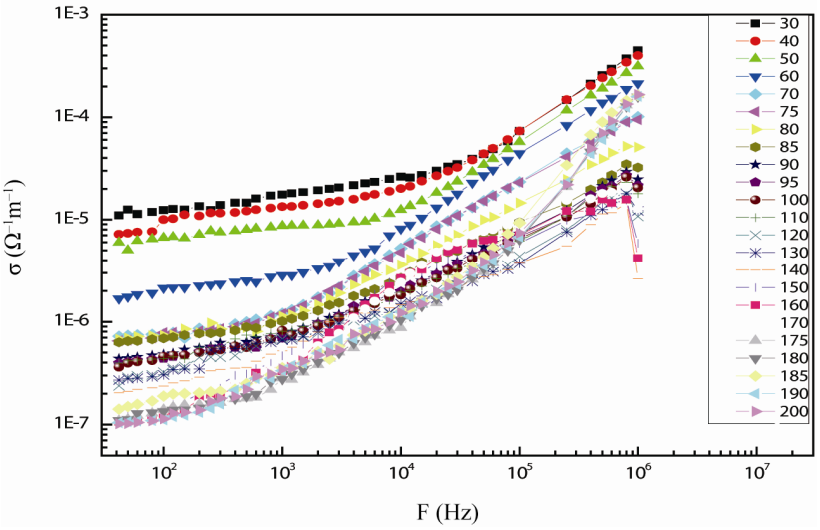

(b)

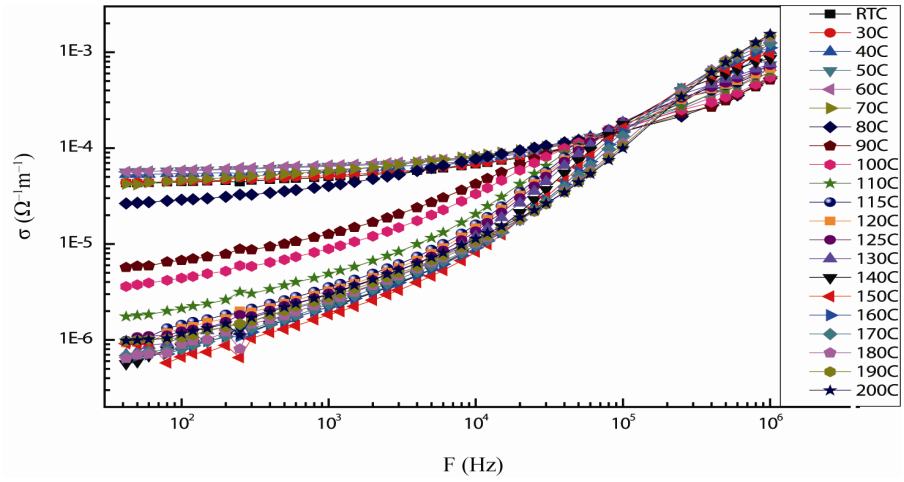

(c)

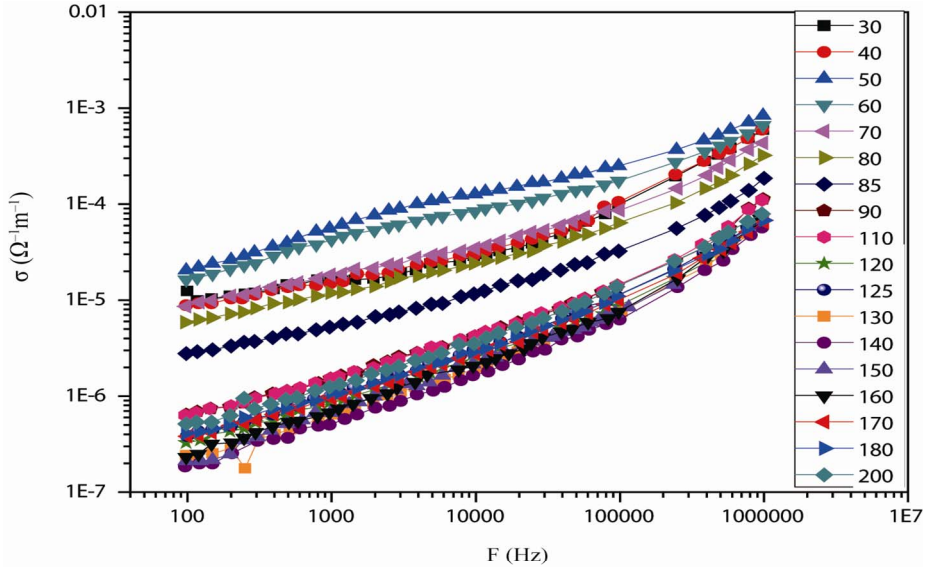

(d)

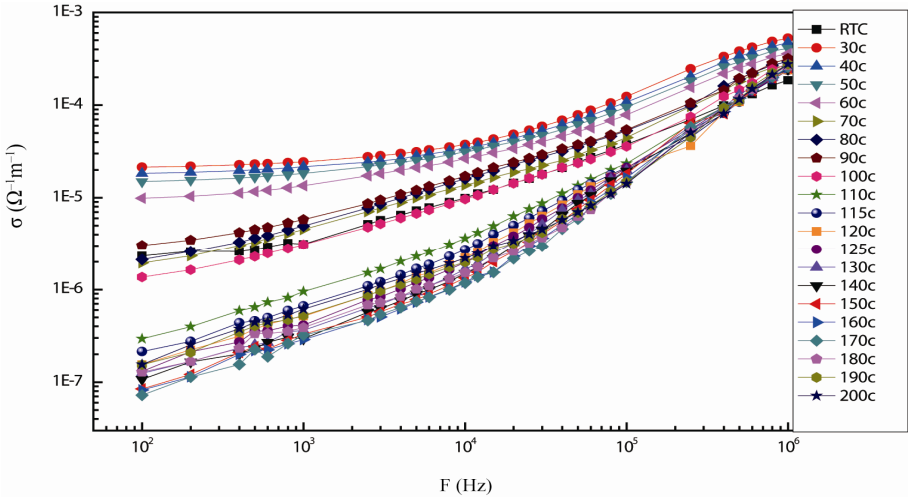

(e)

Figure 9. The A.C. conductivity of (a) B10ST1F; (b) B10ST5F; (c) B10ST10F; (d) B10ST20F and (e) B10ST.

Table 1. The A.C. conductivity of B10ST, B15ST, B10ST5F, B10ST10F and B10ST20F at 3 different temperature 30˚C, 100˚C and 120˚C.

	$\sigma(\Omega)^{-1}cm^{-1}$		
	RTC (30)˚C		
	1 KHz	10 KHz	50 KHz
B10ST	2.44E–05	3.77E–05	7.83E–05
B15ST	6.98E–06	1.05E–05	1.96E–05
B10ST5F	1.76E–05	2.63E–05	4.35E–05
B10ST20F	1.64E–05	2.63E–05	3.84E–05
	RTC 100˚C		
	1 KHz	10 KHz	50 KHz
B10ST	3.10E–06	9.67E–06	2.38E–05
B15ST	1.20E–05	2.29E–05	3.20E–05
B10ST5F	8.25E–07	1.81E–06	4.50E–06
B10ST20F	1.37E–06	3.82E–06	7.89E–06
	RTC 120˚C		
	1KHz	10KHz	50KHz
B10ST	5.12E–07	2.24E–06	1.09E–05
B15ST	1.77E–06	1.08E–05	3.46E–05
B10ST5F	6.78E–07	1.37E–06	3.21E–06
B10ST20F	8.38E–07	2.42E–06	5.46E–06

4. Conclusion

Using the sol-gel method, nano-structure pure B(3, 5 & 20)ST and doped B10ST(1-20)F powder systems have been successfully prepared. Tetragonal phase with unwanted amount of $BaCO_3$ and $SrCO_3$ have been obtained for both the pure and doped with 5 and 20 mol% of iron oxide systems. In addition a well defined perovskite phase with nano-crystallite sizes for B10ST, B10ST5F and B10ST20F equal to 36.5, 33.5 and 32 nm, respectively were achieved. Doping the prepared samples with different concentrations of iron oxide is effective to decrease the crystallite size. TEM micrograph has used to confirm and complement the XRD results giving the following crystallite size value 29.82 nm for B10ST20F. The dielectric properties of both BST and BSTF systems in the ferroelectric phase showed strongly frequency and temperature dependence. At 30˚C the A.C. conductivity was found to decrease by increasing both the Sr concentration from 10 up to 15 mol%, and the iron oxide concentrations from 5 up to 20 mol%, due to the decrease in the grain size and hence the increase in the grain boundary areas/resistance with Sr and Fe substitution.

REFERENCES

[1] I. K. Battisha, A. B. Abou Hamad and R. M. Mahani, "Structure and Dielectric Studies of Nano-Composite Fe_2O_3: $BaTiO_3$ Prepared by Sol-Gel Method," *Physica B*, Vol. 404, No. 16, 2009, pp. 2274-2279. doi:10.1016/j.physb.2009.04.038

[2] F. Lin and W. Shi, "Effect of Sr Concentration on Microstructure and Magnetic Properties of $(Ba_{1-x}Sr_x)(Ti_{0.3}Fe_{0.7})O_3$ Ceramics," *Journal of Magnetism and Magnetic Materials*, Vol. 322, No. 14, 2010, pp. 2081-2085. doi:10.1016/j.jmmm.2010.03.004

[3] X. Wei, G. Xu, Z. Ren, Y. Wang, G. Shen and G. Han, "Size-Controlled Synthesis of $BaTiO_3$ Nanocrystals via a Hydrothermal Route," *Materials Letters*, Vol. 62, No. 21-22, 2008, pp. 3666-3669.

[4] A. Sundaresan and C. N. R. Rao, "Ferromagnetism as a Universal Feature of Inorganic Nanoparticles," *Nano Today*, Vol. 4, No. 1, 2009, pp. 96-106. doi:10.1016/j.nantod.2008.10.002

[5] H. I. Hsing, C. S. Hsib, C. C. Huang and S. L. Fu, "Low Temperature Sintering and Dielectric Properties of $BaTiO_3$ with Glass Addition" *Materials Chemistry and Physics*, Vol. 113, No. 2-3, 2009, pp. 658-663.

doi:10.1016/j.matchemphys.2008.08.033

[6] L. B. Kong, T. S. Zhang, J. Ma and F. Boey, "Progress in Synthesis of Ferroelectric Ceramic Materials Via High-Energy Mechanochemical Technique" *Progress in Materials Science*, Vol. 53, No. 2, 2008, pp. 207-322. doi:10.1016/j.pmatsci.2007.05.001

[7] M. Roscher, T. Schneller, R. Waser, J. Sol-Gel Sci. Tech., Vol. 56, 2010, pp. 236.

[8] Z. Shao, G. Xiong, J. Tong, H. Dong, W. Yang, "Ba Effect in Doped $Sr(Co_{0.8}Fe_{0.2})O_3$-δ on the Phase Structure and Oxygen Permeation Properties of the Dense Ceramic Membranes," *Separation and Purification Technology*, Vol. 25, No. 1-3, 2001, pp. 419-429. doi:10.1016/S1383-5866(01)00071-5

[9] C. Mao, X. Dong, T. Zeng, H. Chen, F. Cao, Ceramics International, Vol. 34, 2008, pp. 45.

[10] R. Kavian and A. Saidi, "Sol-Gel Derived $BaTiO_3$ Nano-Powders," *Journal of Alloys and Compounds*, Vol. 468, No. 1-2, 2009, pp. 528-532. doi:10.1016/j.jallcom.2008.01.045

[11] W. Li, Z. Xu, R. Chu, P. Fu, J. Hao, *Journal of Alloys and Compounds*, Vol. 482, 2009, p. 137.

[12] W. L. Liu, D. Xuea, H. Kanga, C. Liu, "Wet Routes of High Purity $BaTiO_3$ Nanopowders," *Journal of Alloys and Compounds*, Vol. 440, No. 1-2, 2007, pp. 78-83. doi:10.1016/j.jallcom.2006.09.023

[13] B. Fournaud, S. Rossignol, J. M. Tatibou and S. Thollonb, "Spherical Pellets of $BaTiO_3$ and $Ba_{0.67}Sr_{0.33}TiO_3$ Perovskite-Type Compounds Made by a Sol-Gel Oil Drop Process for Non-Thermal Plasma Applications," *Journal of Materials Processing Technology*, Vol. 209, No. 5, 2009, pp. 2515-2521. doi:10.1016/j.jmatprotec.2008.05.046

[14] L. B. Kong, T. S. Zhang, J. Ma and F. Boey, "Progress in Synthesis of Ferroelectric Ceramic Materials via High-Energy Mechanochemical Technique," *Progress in Materials Science*, Vol. 53, No. 2, 2008, pp. 207-322. doi:10.1016/j.pmatsci.2007.05.001

[15] X. H. Zuo, X. Y. Deng, Y. Chen, M. Ruan, W. Li, B. Liu, Y. Qu and B. Xu, "A Novel Method for Preparation of Barium Strontium Titanate Nanopowders," *Materials Letters*, Vol. 64, No. 10, 2010, pp. 1150-1153. doi:10.1016/j.matlet.2010.02.034

[16] R.M. Mahani, I. K. Battisha, and M. A. Salem and A. B. Abou Hamad, "Structure and Dielectric Behavior of Nano-Structure Ferroelectric $Ba_xSr_{1-x}TiO_3$ Prepared by Sol-Gel Method," *Journal of Alloys and Compounds*, Vol. 508, No. 2, 2010, pp. 354-358. doi:10.1016/j.jallcom.2010.05.060

[17] W. Li, Z. Xu, R. Chu, P. Fu and J. Hao, "Sol-Gel Synthesis and Characterization of $Ba_{(1-x)}Sr_xTiO_3$ Ceramics," *Journal of Alloys and Compounds*, Vol. 499, No. 2, 2010, pp. 255-258. doi:10.1016/j.jallcom.2010.03.180

[18] S. B. Deshpandea, Y. B. Khollamb, S. V. Bhoraskarb, S. K. Dateb, S. R. Sainkara and H. S. Potdara, "Synthesis and Characterization of Microwave-Hydrothermally Derived $Ba_{1-x}Sr_xTiO_3$ Powders," *Materials Letters*, Vol. 59, No. 2-3, 2005, pp. 293-296. doi:10.1016/j.matlet.2004.10.006

[19] J. Gong, J. Cheng, W. Zhu, S. Yu, W. Wu and M. Zhongyan, *IEEE*, Vol. 54, No. 12, 2005, pp. 2579.

[20] X. Wei, G. Xu, Z. Ren, Y. Wang, G. Shen and G. Han, "Size-Controlled Synthesis of $BaTiO_3$ Nanocrystals via a Hydrothermal Route," *Materials Letters*, Vol. 62, No. 21-22, 2008, pp. 3666-3669. doi:10.1016/j.matlet.2008.04.022

[21] M. Y. El-Naggar, K. Dayal, D. G. Goodwin and K. Bhattacharya, "Graded Ferroelectric Capacitors with Robust Temperature Characteristics," *Journal of Applied Physics*, Vol. 100, 2006, p. 114115. doi:10.1063/1.2369650

[22] S. U. Adikary and H. L. W. Chan, "Compositionally Graded $Ba_xSr_{1-x}TiO_3$ Thin Films for Tunable Microwave Applications," *Materials Chemistry and Physics*, Vol. 79, No. 2-3, 2003, pp. 157-160. doi:10.1016/S0254-0584(02)00255-9

[23] H. T. Su, M. J. Lancaster, F. Huang, F. Wellh¨ofer, Microwave Opt. Technol. Lett., Vol. 24, 2000, pp. 155.

[24] K.-C. Tsai, W.-F. Wu, C.-G. Chao, J.-T. Lee and S.-W. Shen, "Improving Electrical Properties and Thermal Stability of $(Ba,Sr)TiO_3$ Thin Films on Cu(Mg) Bottom Electrodes," *Japan Journal of Applied Physics*, Vol. 45, 2006, pp. 5495-5500. doi:10.1143/JJAP.45.5495

[25] G. Subramanyam, F. Ahamed and R. Biggers, "A Si MMIC Compatible Ferroelectric Varactor Shunt Switch for Microwave Applications," *IEEE Microwave and Wireless Components Letters*, Vol. 15, No. 11, 2005, pp. 739-741. doi:10.1109/LMWC.2005.858992

[26] J. G. Cheng, J. Tang, J. H. Chu and A. J. Zhang, "Pyroelectric Properties in Sol-Gel Derived Barium Strontium Titanate Thin Films Using a Highly Diluted Precursor Solution," *Applied Physics Letters*, Vol. 77, No. 7, 2000, p. 1035. doi:10.1063/1.1289038

[27] L. Radhapiyari, O. P. Thakur and C. Prakash, "Structural and Dielectric Properties of the System $Ba_{1-x}Sr_xFe_{0.01}Ti_{0.99}O_3$," *Materials Letters*, Vol. 57, No. 12, 2003, pp. 1824-1829. doi:10.1016/S0167-577X(02)01075-3

[28] C. L. Fu, C. R. Yang, H. W. Chen, Y. X. Wang and L. Y. Hu, "Microstructure and Dielectric Properties of $Ba_x Sr_{1-x}TiO_3$ Ceramics," *Materials Science and Engineering*: *B*, Vol. 119, No. 2, 2005, pp. 185-188. doi:10.1016/j.mseb.2005.02.056

[29] [29] T. Matsuoka, Y. Matsuo, H. Sasaki and S. Hayakawa, "PTCR Behavior of $BaTiO_3$ with Nb_2O_5 and MnO_2 Additives," *Journal of the American Ceramic Society*, Vol. 55, No. 2, 1972, p. 108. doi:10.1111/j.1151-2916.1972.tb11223.x

[30] N. H. Chan and D. M. Smyth, "Defect Chemistry of $BaTiO_3$" *Journal of Electrochemical Society*, Vol. 123, No. 10, 1976, pp. 1584-1585. doi:10.1149/1.2132644

